BIOCHEMISTRY
including biophysical chemistry & molecular biology

Article

pubs.acs.org/biochemistry

Thermal Stability of DNA Quadruplex–Duplex Hybrids

Kah Wai Lim,[†,‡,§] Zi Jian Khong,[†,§] and Anh Tuân Phan*[,†]

[†]School of Physical and Mathematical Sciences, Nanyang Technological University, Singapore 637371

[‡]School of Biological Sciences, Nanyang Technological University, Singapore 637551

Supporting Information

ABSTRACT: DNA has the capacity to adopt several distinct structural forms, such as duplex and quadruplex helices, which have been implicated in cellular processes and shown to exhibit important functional properties. Quadruplex–duplex hybrids, generated from the juxtaposition of these two structural elements, could find applications in therapeutics and nanotechnology. Here we used NMR and CD spectroscopy to investigate the thermal stability of two classes of quadruplex–duplex hybrids comprising fundamentally distinct modes of duplex and quadruplex connectivity: Construct I involves the coaxial orientation of the duplex and quadruplex helices with continual base stacking across the two components; Construct II involves the orthogonal orientation of the duplex and quadruplex helices with no base stacking between the two components. We have found that for both constructs, the stability of the quadruplex generally increases with the length of the stem–loop incorporated, with respect to quadruplexes comprising nonstructured loops of the same length, which showed a continuous drop in stability with increasing loop length. The stability of these complexes, particularly Construct I, can be substantially influenced by the base-pair steps proximal to the quadruplex–duplex junction. Bulges at the junction are largely detrimental to the adoption of the desired G-quadruplex topology for Construct I but not for Construct II. These findings should facilitate future design and prediction of quadruplex–duplex hybrids.

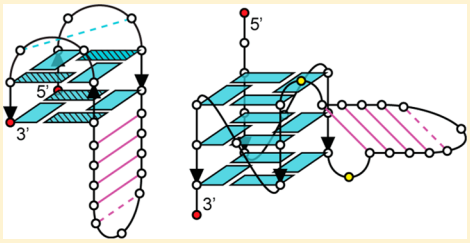

The canonical conformation of DNA is the B-form duplex, which consists of two antiparallel right-handed helical strands held together by Watson–Crick base pairs (bp). On the other hand, the G-quadruplex[1−3] is a four-stranded helical assembly made up of multiple stacked G·G·G·G tetrads[4] stabilized by Hoogsteen hydrogen bonds.[5] G-quadruplexes can adopt a diverse range of structures: the four strands making up the core can be arranged in four different relative orientations; the linkers (or loops) can connect the four strands in different manners; and the G-tetrad core can consist of two or more tetrad layers.[3] We recently presented a systematic analysis of the incorporation of a duplex stem across the various geometries of a quadruplex core,[6] demonstrating the facile juxtaposition of these two structural elements. It is thus important to establish thermodynamic descriptions regarding their conjointment, as that would facilitate future design and prediction of quadruplex–duplex hybrids,[6−11] which could find applications in therapeutics and nanotechnology.

Previous thermodynamic studies[12,13] on quadruplexes comprising loops of varying compositions shed light on the effects of the loop length and sequence on the quadruplex conformation and stability.[14−22] A loop consisting of a single nucleotide shows a propensity toward the propeller (or double-chain-reversal) configuration[14,15,17,20] and is especially stable. In addition, an increase in loop length seems to reduce the stability of a quadruplex.[14,15,18−20,22] However, the long loops that have been investigated do not contain any explicit stabilizing interactions, which could have been the cause of their destabilizing nature. Here we set out to determine the effects of stem–loop incorporation on quadruplex stability.[11] To this end, two classes of quadruplex–duplex hybrids with contrasting orientations of the duplex stem with respect to the tetrad core were investigated. Using NMR[23] and CD[24] spectroscopy, we outline the influences that stem–loop length and its sequence, particularly the base-pair steps proximal to the junction, exert on the stability of these complexes. We also highlight the consequences of having bulges at the quadruplex–duplex junction.

MATERIALS AND METHODS

DNA Sample Preparation. DNA oligonucleotides were chemically synthesized on an ABI 394 DNA/RNA synthesizer using products from Glen Research. The oligonucleotides were deprotected following the manufacturer's protocols and purified using Poly-Pak cartridges. Samples were dialyzed successively against water, 10 mM KCl solution, and water again. They were subsequently frozen, lyophilized, and suspended in a buffer containing 10 mM lithium phosphate (pH 7.0) and 10 mM KCl. DNA concentration is expressed as strand molarity using a nearest-neighbor approximation for the absorption coefficients of the unfolded species,[25] based on 260-nm molar extinction coefficients provided by the "UV Spectrum of DNA" online application (http://biophysics.idtdna.com/UVSpectrum.html).

Received: August 23, 2013
Revised: December 6, 2013
Published: December 24, 2013

NMR Spectroscopy. 1D NMR experiments were performed on a Bruker AVANCE 600 MHz spectrometer at 25 °C using JR-type pulse sequences for water signal suppression.

Circular Dichroism. Unless otherwise stated, circular dichroism (CD) spectra were recorded at 25 °C on a JASCO-815 spectropolarimeter over the range of 220−320 nm using a 1-cm path length quartz cuvette with a reaction volume of 500 μL. The DNA concentration was typically 4 μM. For each sample, an average of three scans was taken, the spectrum of the buffer was subtracted, and the data were zero-corrected at 320 nm. For CD melting experiments, cooling and heating were successively performed across the temperature range of 15−95 °C over a total of 14 h. The full spectrum was recorded at intervals of 1 °C, after which the molar ellipticity at the appropriate wavelength was extracted (295 nm for Construct I; 262 nm for Construct II). Two baselines corresponding to the completely folded (low temperature) and completely unfolded (high temperature) states were manually drawn in order to determine the fractions of folded and unfolded species during the melting process. The melting temperature (T_m) is defined as the temperature for which there are equal fractions of folded and unfolded species. For each sequence, the average T_m from the folding and unfolding experiments is presented. The difference between the T_m values from the folding and unfolding experiments for all quadruplex−duplex hybrids was less than 1.2 °C. For clarity, only the folding curves are presented in the main text.

RESULTS

Design of Quadruplex−Duplex Hybrids. The series of duplex stems (Table 1) and quadruplex−duplex hybrids (Tables 2 and 3) investigated were based on structures elucidated previously.[6] Construct I consists of a chair-type G-quadruplex,[26] in which the duplex stem is adjoined to the tetrad core across the wide groove through continuous base stacking[6] (Figure 1A). Construct II consists of an all-parallel-stranded G-quadruplex,[27,28] wherein the duplex stem projects laterally outward from the tetrad core as the middle propeller loop[6] (Figure 1B). To discount variations arising from the hairpin end distal from the quadruplex−duplex junction, the same GCA hairpin loop[29] was incorporated across all sequences. For Construct II, a linker residue was added onto each of the two points of contact between the duplex and the quadruplex on the basis of prior knowledge that a base pair at this junction type would have to be broken up upon complex formation.[6] The length and sequence of the duplex stem were varied in a systematic manner for both constructs. Bulges[30,31] were further introduced at the quadruplex−duplex junction to determine the effects that they exert on the adoption of the desired G-quadruplex topologies. In all cases, both NMR and CD spectroscopy were employed to inspect the topologies of the oligonucleotides.

Table 1. Sequences of Reference Duplex Hairpins Used in This Study

Name	Sequence
3bp	CGC GCA GCG
4bp	CGCG GCA CGCG
5bp	CGCGA GCA TCGCG
6bp	CGCGAA GCA TTCGCG
11bp	CGCGAATCTGT GCA ACAGATTCGCG
11bp[CG]	CGCGCGCGCGC GCA GCGCGCGCGCG
16bp	CGCGAATCTGTGATAC GCA GTATCACAGATTCGCG

NMR and CD Validation of Quadruplex−Duplex Hybrids with Variable Stem Length. The 1D proton NMR spectra of the skeletal structures of Constructs I and II containing no duplex stem (denoted as *W2C-0bp* in Table 2 and *M2C-0bp* in Table 3, respectively) indicated the presence of a single conformation. *W2C-0bp* showed 10 imino proton peaks at ∼11−12.4 ppm (Figure 2B), consistent with the adoption of a two-tetrad G-quadruplex with a capping T·T base pair.[26] *M2C-0bp* displayed 12 imino proton peaks at ∼11−12.1 ppm (Figure 2D), consistent with the formation of a three-tetrad G-quadruplex.[27,28] In contrast, the imino protons of Watson−Crick base pairs typically appear at ∼12−14 ppm (Figure S1 in the Supporting Information), as is evident from the spectrum of a reference duplex stem with six base pairs (denoted as *dx-6bp*; Table 1 and Figure 2A). Incorporation of the same duplex stem in the respective quadruplex constructs (giving *W2C-6bp* and *M2C-6bp*, respectively; Tables 2 and 3) yielded quadruplex−duplex hybrids with the expected topologies; the quadruplex−duplex hybrids displayed imino proton peaks in both chemical shift ranges of duplexes and quadruplexes, and the peak distribution patterns resembled those of the individual duplex and quadruplex components (Figure 2C,E). For *W2C-6bp*, an additional imino proton peak was observed at 13.2 ppm, corresponding to the base pair of the duplex stem at the quadruplex−duplex junction, that is protected from exchange with solvent. Complexes with a stem length of up to 16 base pairs were investigated for both constructs (Tables 2 and 3). For the oligonucleotides harboring a duplex stem with two or more base pairs, the duplex peaks built up incrementally as the number of base pairs was increased while the quadruplex peaks retained similar distribution patterns (Construct I, Figure 3; Construct II, Figure 4), indicating that these quadruplex−duplex hybrids adopted the desired topologies as the predominant conformation.

The CD spectra of the oligonucleotides supported their adoption of the desired topologies. The CD spectrum of *dx-6bp* displayed a peak at ∼275 nm and a trough at ∼250 nm (Figure 5A, orange), approximating that of a related duplex.[32] *W2C-0bp* showed two positive maxima around 245 and 290−295 nm (Figure 5A, green), typical of a chair-type G-quadruplex.[24,33] *M2C-0bp* exhibited a maximum at 262 nm and a negative minimum at around 240 nm (Figure 5A, violet), characteristic of an all-parallel-stranded G-quadruplex.[15,24,27,28] The CD spectra of the quadruplex−duplex hybrids (Figures S2 and S3 in the Supporting Information) corresponded well with the sum of their component duplex (Figure S4 in the Supporting Information) and quadruplex spectra, as exemplified by *W2C-6bp* (Figure 5B) and *M2C-6bp* (Figure 5C).

CD Melting Experiments on Duplex, Quadruplex, and Quadruplex−Duplex Hybrids. CD melting experiments on *dx-6bp*, *W2C-0bp*, and *M2C-0bp* were first performed. *dx-6bp* showed considerable variations at around 250 and 270 nm, and there was minimal change at ∼262 nm (Figure 6A). *W2C-0bp* displayed a large change at ∼290−295 nm and minimal changes at around 250 and 275 nm (Figure 6B). *M2C-0bp* displayed the largest variation at 262 nm and almost no variation at around 250 nm (Figure 6C). Previous studies suggested that the peak at ∼260 nm is indicative of quadruplexes in which adjacent tetrads are aligned with the same hydrogen-bond directionality,

Table 2. Sequences of Construct I (*W2C*) Used in This Study

	Name	Sequence[a,b]			T_m[c] (°C)
Duplex Stem Length/ Sequence Variation	*0bp*	GGTTGG	GCA	GGTTGG	36.2
	1bp	GGTTGG	C GCA G	GGTTGG	39.0[d]
	2bp	GGTTGG	CG GCA CG	GGTTGG	38.2
	3bp	GGTTGG	CGC GCA GCG	GGTTGG	41.6
	4bp	GGTTGG	CGCG GCA CGCG	GGTTGG	43.0
	5bp	GGTTGG	CGCGA GCA TCGCG	GGTTGG	43.5
	6bp	GGTTGG	CGCGAA GCA TTCGCG	GGTTGG	42.6
	11bp	GGTTGG	CGCGAATCTGT GCA ACAGATTCGCG	GGTTGG	43.9
	11bp[CG]	GGTTGG	CGCGCGCGCGC GCA GCGCGCGCGCG	GGTTGG	44.6
	16bp	GGTTGG	CGCGAATCTGTGATAC GCA GTATCACAGATTCGCG	GGTTGG	43.7
Loop Length Reference	*1T*	GGTTGG	T	GGTTGG	–[e]
	2T	GGTTGG	TT	GGTTGG	–[e]
	3T	GGTTGG	TTT	GGTTGG	–[e]
	5T	GGTTGG	TTTTT	GGTTGG	–[e]
	15T	GGTTGG	T_{15}	GGTTGG	–[e]
	25T	GGTTGG	T_{25}	GGTTGG	–[e]
	35T	GGTTGG	T_{35}	GGTTGG	–[e]
Base Pair Variation/ Bulge at Junction	*6bp[G7/C21]*	GGTTGG	GGCGAA GCA TTCGCC	GGTTGG	35.4
	6bp[T7/A21]	GGTTGG	TGCGAA GCA TTCGCA	GGTTGG	32.2
	6bp[A7/T21]	GGTTGG	AGCGAA GCA TTCGCT	GGTTGG	36.5
	6bp[C8/G20]	GGTTGG	CCCGAA GCA TTCGGG	GGTTGG	45.7
	6bp[T8/A20]	GGTTGG	CTCGAA GCA TTCGAG	GGTTGG	43.2
	6bp[A8/T20]	GGTTGG	CACGAA GCA TTCGTG	GGTTGG	42.1
	6bp[+T7]	GGTTGG	**T**CGCGAA GCA TTCGCG	GGTTGG	–[e]
	6bp[+T21]	GGTTGG	CGCGAA GCA TTCGCG**T**	GGTTGG	–[e]
	6bp[+T7/+T22]	GGTTGG	**T**CGCGAA GCA TTCGCG**T**	GGTTGG	24.5[d]

[a]Base pair variations near the junction are underlined. [b]Bulges are shown in boldface. [c]Melting temperatures in 10 mM K^+ solution, as monitored by the molar ellipticity at 295 nm. [d]This melting temperature consists of considerable contributions from additional conformation(s). [e]The melting temperature of this oligonucleotide was not determined because the desired quadruplex topology was not observed as a major form by NMR.

whereas the peak at ~295 nm reflects quadruplexes in which adjacent tetrads possess alternate polarities.[34] The large variation shown by *W2C-0bp* at 295 nm coincides with a region of minimal change for *dx-6bp*, making this wavelength ideal for tracing the melting of the quadruplex segment of Construct I. Following the same logic, the melting process of the quadruplex segment of Construct II could be monitored readily at 262 nm. Subsequent melting analyses of the quadruplex–duplex hybrids were carried out for only the quadruplex segments of Constructs I and II at 295 and 262 nm, respectively. Signal variations at these two wavelengths for the series of reference duplex hairpins were minimal as compared to those for the quadruplex core (Figure S5 in the Supporting Information). Hence the melting temperatures determined at these two particular wavelengths should give a fair estimate of the stabilities of the respective quadruplex components. It should be noted that for quadruplex–duplex hybrids with different sequence compositions of the duplex stem, monitoring the changes at alternative wavelengths might have been more suitable.

Effects of Duplex Stem Length and Sequence on the Stability of Quadruplex–Duplex Hybrids. Folding curves for Construct I and Construct II with variable duplex stem lengths were derived from the molar ellipticities at 295 and 262 nm, respectively (Figure 7). The melting temperature of Construct I increased from 36.2 °C without any Watson–Crick base pairs to 41.6 °C with three Watson–Crick base pairs, eventually leveling off at 41–44 °C at longer duplex stem lengths (Table 2 and Figure 7A). The melting temperature of Construct II showed a marginal increase from 62.2 °C without any Watson–Crick base pair to ~63–65 °C at intermediate duplex stem lengths with three to six Watson–Crick base pairs, followed by a modest increase to ~66.5 °C at long duplex stem lengths (Table 3 and Figure 7B). This is in stark contrast to the trend observed for Construct II comprising nonstructured loops [i.e., poly(dT)], which showed a continuous decrease in melting temperature with increasing loop length[14,15,18–20,22] (from 63.8 °C at T_5 to 41.6 °C at T_{37}) (Table 3 and Figures S6 and S7 in the Supporting Information). Similar comparisons for Construct I could not be made, as the desired quadruplex topology was no longer the major form with a nonstructured loop as short as five nucleotides (Table 2 and Figure S8 in the Supporting Information). The oligonucleotides containing an 11-bp duplex stem were modified to explore the extent to which sequence changes in the duplex stem can affect their stability; modification of the 11-bp duplex stem to poly[d(CG)] led to an increase in melting temperature of ~1 °C for both quadruplex–duplex constructs (Tables 2 and 3 and Figure S9 in the Supporting Information).

Effects of Base-Pair Composition at the Junction on the Stability of Quadruplex–Duplex Hybrids. The base-pair step from the 6-bp stem immediately adjoining the quadruplex–duplex junction (i.e., C7·G21 for *W2C-6bp* and C11·G25 for *M2C-6bp*) was substituted like-for-like (with G·C,

dx.doi.org/10.1021/bi401161a | *Biochemistry* 2014, 53, 247–257

Table 3. Sequences of Construct II (*M2C*) Used in This Study

	Name	Sequence[a,b]	T_m[c] (°C)
Duplex Stem Length/ Sequence Variation	*0bp*	TTGGGTGGG **T** GCA **T** GGGTGGGT	62.2
	1bp	TTGGGTGGG **T**C GCA G**T** GGGTGGGT	60.9
	2bp	TTGGGTGGG **T**CG GCA CG**T** GGGTGGGT	60.8
	3bp	TTGGGTGGG **T**CGC GCA GCG**T** GGGTGGGT	65.3
	4bp	TTGGGTGGG **T**CGCG GCA CGCG**T** GGGTGGGT	64.4
	5bp	TTGGGTGGG **T**CGCGA GCA TCGCG**T** GGGTGGGT	63.6
	6bp	TTGGGTGGG **T**CGCGAA GCA TTCGCG**T** GGGTGGGT	63.0
	11bp	TTGGGTGGG **T**CGCGAATCTGT GCA ACAGATTCGCG**T** GGGTGGGT	66.6
	11bp[CG]	TTGGGTGGG **T**CGCGCGCGCGC GCA GCGCGCGCGCG**T** GGGTGGGT	67.9
	16bp	TTGGGTGGG **T**CGCGAATCTGTGATAC GCA GTATCACAGATTCGCG**T** GGGTGGGT	66.8
Loop Length Reference	*1T*	TTGGGTGGG T GGGTGGGT	83.2
	2T	TTGGGTGGG TT GGGTGGGT	76.5
	3T	TTGGGTGGG TTT GGGTGGGT	70.7
	[T]3T[T]	TTGGGTGGG **T**T_3**T** GGGTGGGT	63.8
	[T]5T[T]	TTGGGTGGG **T**T_5**T** GGGTGGGT	59.2
	[T]7T[T]	TTGGGTGGG **T**T_7**T** GGGTGGGT	56.6
	[T]9T[T]	TTGGGTGGG **T**T_9**T** GGGTGGGT	53.7
	[T]11T[T]	TTGGGTGGG **T**T_{11}**T** GGGTGGGT	51.8
	[T]13T[T]	TTGGGTGGG **T**T_{13}**T** GGGTGGGT	50.8
	[T]15T[T]	TTGGGTGGG **T**T_{15}**T** GGGTGGGT	48.8
	[T]25T[T]	TTGGGTGGG **T**T_{25}**T** GGGTGGGT	42.6
	[T]35T[T]	TTGGGTGGG **T**T_{35}**T** GGGTGGGT	41.6
Base Pair Variation/Bulge at Junction	*6bp[G11/C25]*	TTGGGTGGG **T**G**C**GCGAA GCA TTCGC**C**T GGGTGGGT	63.4
	6bp[T11/A25]	TTGGGTGGG **T**T**A**GCGAA GCA TTCGC**A**T GGGTGGGT	60.2
	6bp[A11/T25]	TTGGGTGGG **T**A**T**GCGAA GCA TTCGC**T**T GGGTGGGT	60.8
	6bp[C12/G24]	TTGGGTGGG **T**C**G**CGAA GCA TTCG**G**GT GGGTGGGT	–[d]
	6bp[T12/A24]	TTGGGTGGG **T**C**A**CGAA GCA TTCG**A**GT GGGTGGGT	–[d]
	6bp[A12/T24]	TTGGGTGGG **T**C**T**CGAA GCA TTCG**T**GT GGGTGGGT	–[d]
	6bp[C10]	TTGGGTGGG **C**CGCGAA GCA TTCGCGT GGGTGGGT	63.0
	6bp[G10]	TTGGGTGGG **G**CGCGAA GCA TTCGCGT GGGTGGGT	63.5
	6bp[A10]	TTGGGTGGG **A**CGCGAA GCA TTCGCGT GGGTGGGT	63.0
	6bp[C26]	TTGGGTGGG **T**CGCGAA GCA TTCGCG**C** GGGTGGGT	62.6
	6bp[G26]	TTGGGTGGG **T**CGCGAA GCA TTCGCG**G** GGGTGGGT	63.9
	6bp[A26]	TTGGGTGGG **T**CGCGAA GCA TTCGCG**A** GGGTGGGT	63.9
	6bp[C10/G26]	TTGGGTGGG **C**CGCGAA GCA TTCGCG**G** GGGTGGGT	62.0
	6bp[G10/C26]	TTGGGTGGG **G**CGCGAA GCA TTCGCG**C** GGGTGGGT	58.6
	6bp[-T10/-T26]	TTGGGTGGG **C**GCGAA GCA TTCGC**G** GGGTGGGT	63.0
	6bp[-T10]	TTGGGTGGG **C**GCGAA GCA TTCGCGT GGGTGGGT	62.5
	6bp[-T26]	TTGGGTGGG **T**CGCGAA GCA TTCGC**G** GGGTGGGT	63.1
	6bp[+T11]	TTGGGTGGG **TT**CGCGAA GCA TTCGCGT GGGTGGGT	62.3
	6bp[+T26]	TTGGGTGGG **T**CGCGAA GCA TTCGCGTT GGGTGGGT	62.3
	6bp[+T11/+T27]	TTGGGTGGG **TT**CGCGAA GCA TTCGCGTT GGGTGGGT	61.3
	6bp[+T11T12]	TTGGGTGGG **TTT**CGCGAA GCA TTCGCGT GGGTGGGT	61.3
	6bp[+T26T27]	TTGGGTGGG **T**CGCGAA GCA TTCGCGTTT GGGTGGGT	61.0
	6bp[+T11T12/+T28T29]	TTGGGTGGG **TTT**CGCGAA GCA TTCGCGTTT GGGTGGGT	59.4

[a]Base pair/bulge variations near the junction are underlined. [b]Bulges are shown in boldface. [c]Melting temperatures in 10 mM K^+ solution, as monitored by the molar ellipticity at 262 nm. [d]The melting temperature of this oligonucleotide was not determined; the desired topology was observed by NMR, but the base-pair variation is not expected to give rise to a significant change in the melting temperature.

T·A, or A·T; Tables 2 and 3) to determine the changes that arise from base-pair variability at the junction. The predominant conformation for both constructs remained the same, as indicated by NMR data (Figures S10 and S11 in the Supporting Information). For Construct I, C·G at the junction led to the highest stability, with a melting temperature of 42.6 °C; G·C and A·T at the junction gave melting temperatures of ∼36 °C, while T·A at the junction resulted in the least stable complex, with a drop in melting temperature exceeding 10 °C when compared against C·G (Table 2). The disparity in stability was less pronounced in the case of Construct II, with C·G and G·C at the junction displaying a slightly higher melting temperatures (∼3 °C) compared with either T·A or A·T (Table 3). Variations of the next base pair step for Construct I was

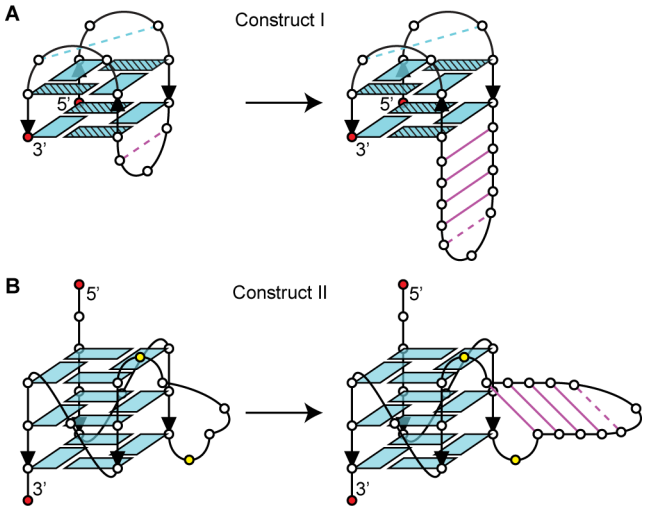

Figure 1. Schematic diagrams illustrating the basis of duplex stem incorporation for (A) Construct I and (B) Construct II. Duplex and quadruplex segments are colored in magenta and cyan, respectively. Guanine bases in the *syn* conformation are shaded. Watson–Crick and noncanonical base pairs are represented as solid and dotted lines, respectively. 5′- and 3′-terminal residues are shown as red circles and bulges as yellow circles.

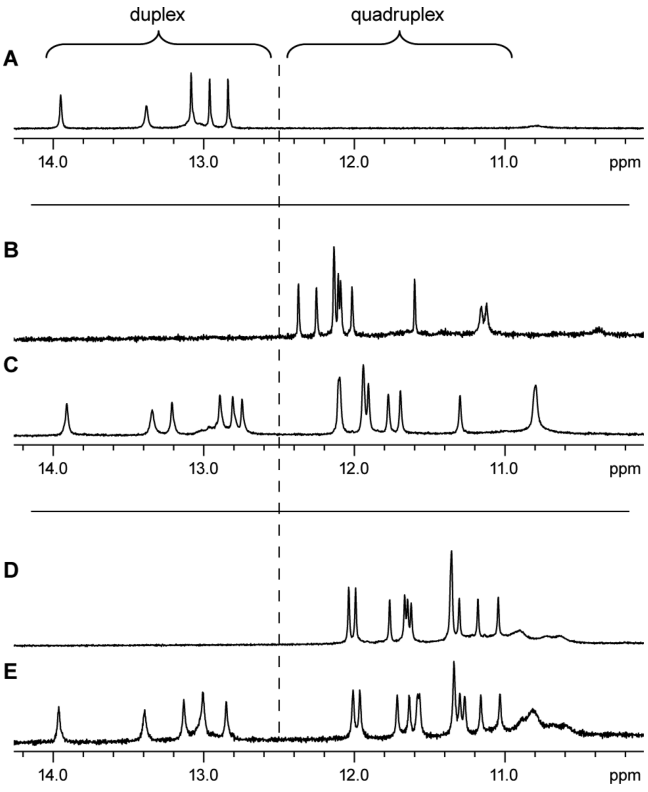

Figure 2. 1D imino proton NMR spectra of representative duplex, quadruplex, and quadruplex–duplex hybrid constructs: (A) the reference duplex stem (*dx-6bp*); (B) Construct I without a duplex stem (*W2C-0bp*); (C) Construct I with the reference duplex stem incorporated (*W2C-6bp*); (D) Construct II without a duplex stem (*M2C-0bp*); (E) Construct II with the reference duplex stem incorporated (*M2C-6bp*).

performed, keeping the C7·G21 base pair intact. Melting temperatures of the three variants were within ~3 °C from that

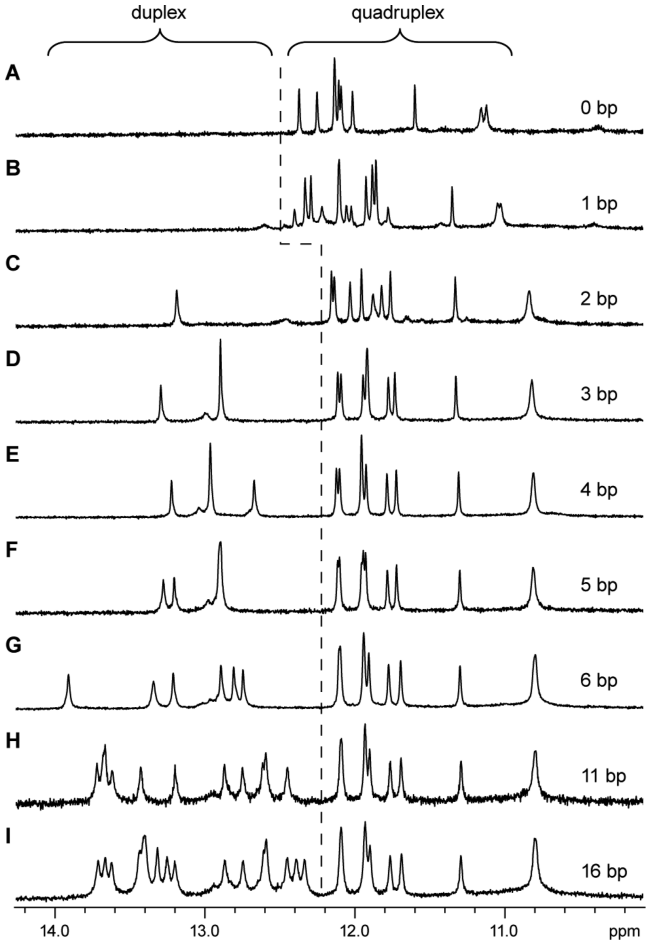

Figure 3. 1D imino proton NMR spectra of Construct I with variable stem length: (A) *W2C-0bp*; (B) *W2C-1bp*; (C) *W2C-2bp*; (D) *W2C-3bp*; (E) *W2C-4bp*; (F) *W2C-5bp*; (G) *W2C-6bp*; (H) *W2C-11bp*; (I) *W2C-16bp*.

of *W2C-6bp* (Table 2). Similar behavior should be expected for their counterparts in Construct II.

Effects of Bulges at the Quadruplex–Duplex Junction. We followed with an investigation of the effects of bulges at the quadruplex–duplex junction (Tables 2 and 3) on the conformation and stability of the resulting complexes. For Construct I, a single bulge at the 5′-side (Figure 8A) or 3′-side (Figure 8B) of the duplex stem adjoining the quadruplex was detrimental to adoption of the desired G-quadruplex topology, with the former posing a more severe effect. The presence of single-nucleotide bulges on both sides of the junction somewhat restored the adoption of the desired G-quadruplex topology (Figure 8C) but led to a drastic drop in stability (~18 °C decrease in melting temperature with respect to *W2C-6bp*; Table 2). On the other hand, for Construct II, there was minimal emergence of minor conformations even with bulges of up to three nucleotides (including the original pair of linker nucleotides) on either/both sides of the junction (Figure 9 and Figure S12 in the Supporting Information). The stability of Construct II comprising bulges of various sizes and sequence compositions did not seem to deviate much from that of *M2C-6bp* (Table 3). This applies even to cases in which the bulge sizes at both sides of the junction are not the same. It should be noted that because of the geometry at the quadruplex–duplex

dx.doi.org/10.1021/bi401161a | *Biochemistry* 2014, 53, 247–257

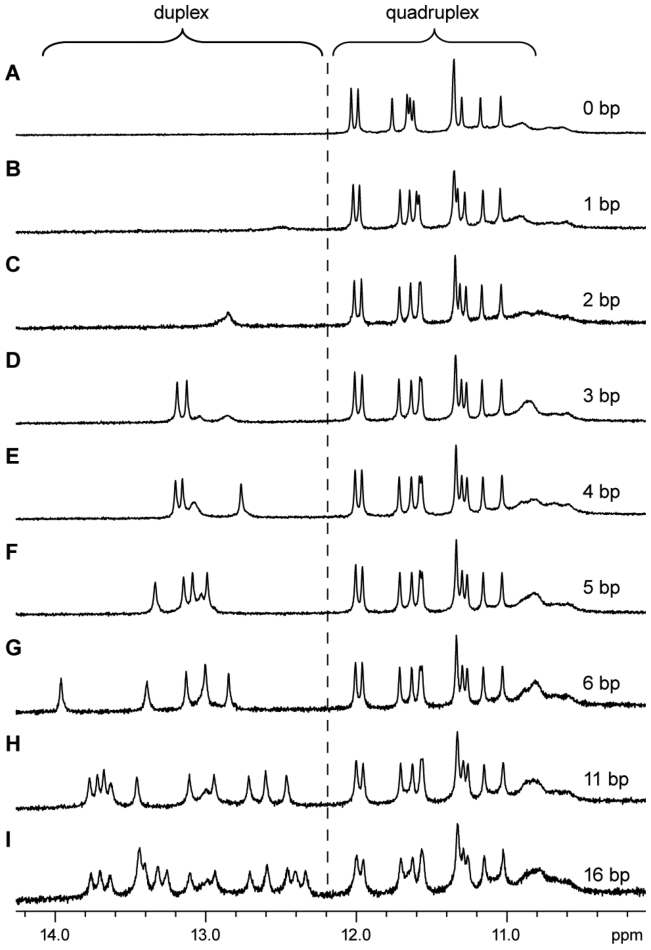

Figure 4. 1D imino proton NMR spectra of Construct II with variable stem length: (A) *M2C-0bp*; (B) *M2C-1bp*; (C) *M2C-2bp*; (D) *M2C-3bp*; (E) *M2C-4bp*; (F) *M2C-5bp*; (G) *M2C-6bp*; (H) *M2C-11bp*; (I) *M2C-16bp*.

junction, Construct II would need to accommodate at least one bulged nucleotide at both sides of the junction.

DISCUSSION

Design and Prediction of Quadruplex–Duplex Hybrids. Previously, we elaborated the compatibility between duplex and quadruplex DNA with the design and structural elucidation of five representative quadruplex–duplex constructs,[6] which brought forward the conceptualization of a myriad of quadruplex–duplex hybrids and G-junction motifs. Here we investigated the thermal stabilities of two representative classes of quadruplex–duplex hybrids: one with continual stacking between the duplex and quadruplex segments (Construct I) and the other with an orthogonal orientation of the duplex stem with respect to the quadruplex core (Construct II). It should be noted that Construct I consists of two G-tetrad layers whereas Construct II consists of three G-tetrad layers, leading to separate ranges for the melting temperatures of the two series of sequences. Nevertheless, the findings should be applicable to quadruplex–duplex hybrids comprising similar arrangements of duplex and quadruplex helices, wherein comparable extents of stabilization should be expected within each junction type. However, quadruplex–duplex hybrids having alternative forms of connectivity at the junction (e.g., with a duplex stem adjoining the diagonal corners of a tetrad) might exhibit different behaviors and would warrant further studies. Insights gained from this study should contribute toward the design and prediction of these motifs (e.g., in the sequence design stage for DNA nanomaterials[35] or in the search for putative quadruplex sequences in the human genome[36,37]).

Duplex Elements Play a Guiding Role in the Establishment of Quadruplex–Duplex Hybrids. G-quadruplexes have been demonstrated to exist in a multitude of conformations.[3] To date, the folding principles governing their formation have not been fully understood. The design of a G-quadruplex folding topology through control over the glycosidic conformations of the guanine bases constituting the tetrad core has been reported previously.[38−43] In a recent study, duplex elements were utilized to preorient three G-rich strands for the induction of a trimolecular G-quadruplex.[44] Similarly, in the development of quadruplex–duplex hybrids, we coupled the integration of duplex stems as quadruplex loops with the strategic placement of auxiliary structural elements to drive G-quadruplex formation toward the desired topology.[6] In the case of Construct I, this involves direct extension of the duplex stem from the tetrad core, as the geometry of the duplex stem matches favorably across the wide groove of the G-quadruplexes. The facile formation of the duplex stem restricts the conformational space that the G-tracts can explore and guides them into the proper spatial orientation whereby the desired topology can then be attained. This guiding role of the

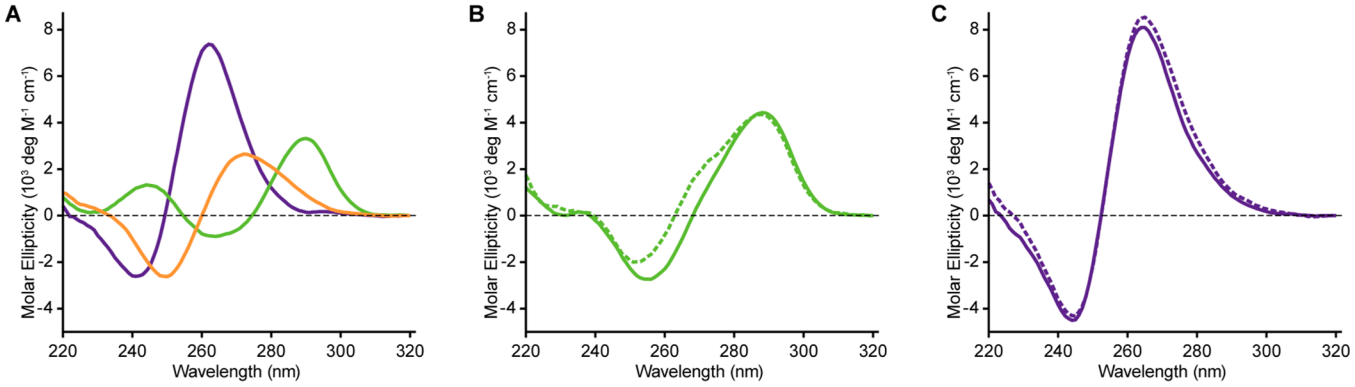

Figure 5. (A) CD spectra of *dx-6bp* (orange), *W2C-0bp* (green), and *M2C-0bp* (violet). (B) The CD spectrum of *W2C-6bp* (solid green line) and the sum of the CD spectra of *W2C-0bp* and *dx-6bp* (dotted green line). (C) The CD spectrum of *M2C-6bp* (solid violet line) and the sum of the CD spectra of *M2C-0bp* and *dx-6bp* (dotted violet line).

dx.doi.org/10.1021/bi401161a | *Biochemistry* 2014, 53, 247−257

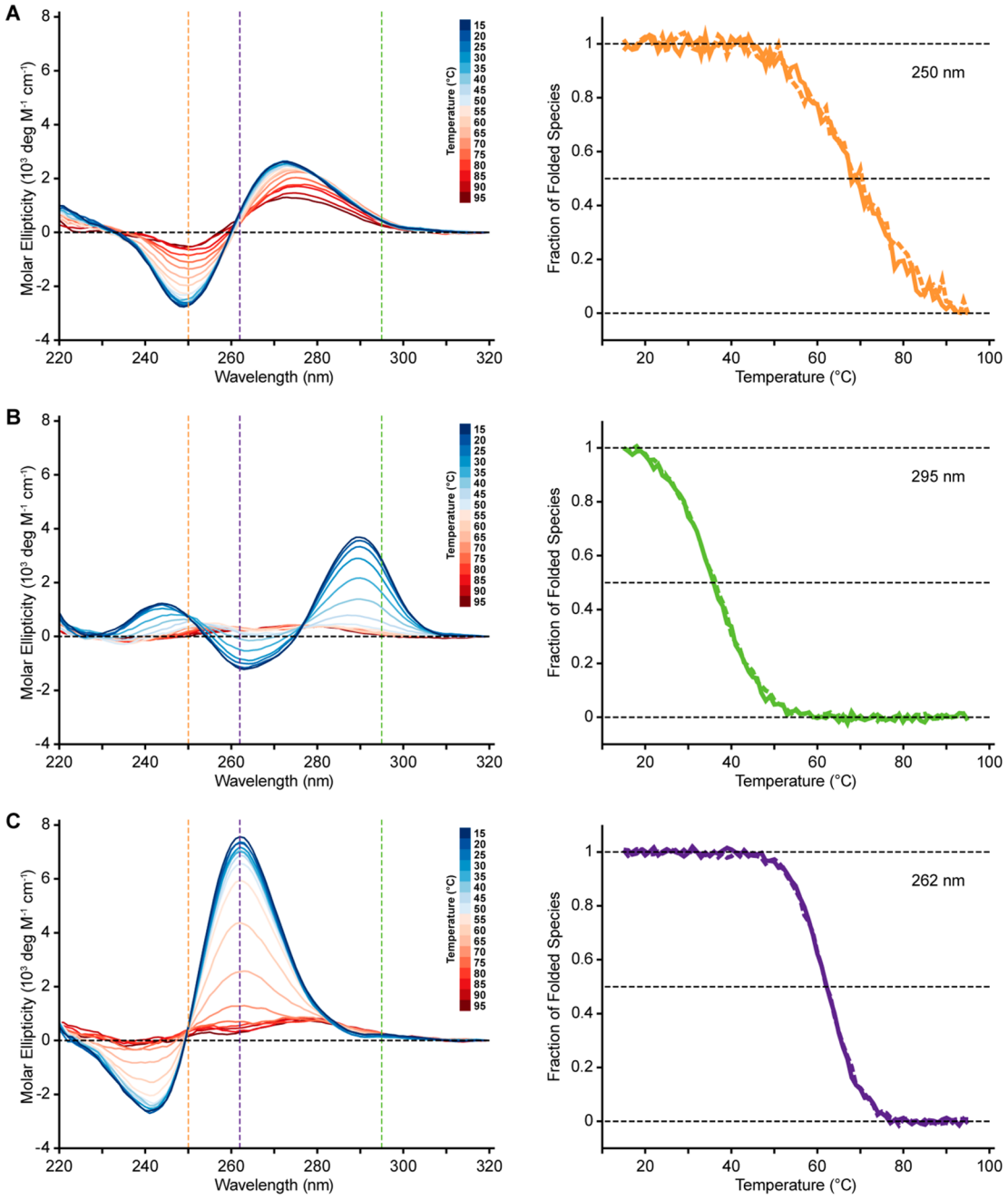

Figure 6. On the left: CD spectra of (A) *dx-6bp*, (B) *W2C-0bp*, and (C) *M2C-0bp* from 15 to 95 °C (color-coded on the top right corners). On the right: Monitoring of the folding/unfolding processes of the different structural forms through the peaks at (A) 250 nm (orange; duplex segment), (B) 295 nm (green; Construct I), and (C) 262 nm (violet; Construct II). Folding and unfolding curves are represented as solid and dotted lines, respectively.

duplex stem substantially contributes toward the adoption of the desired G-quadruplex topology; considerable minor species emerged when a nonstructured loop that was just five nucleotides long was used in place of the duplex stem. In the case of Construct II, the presence of the duplex stem is not as crucial in driving the G-quadruplex to a single topology, presumably because the GGGTGGG motif has an extreme preference to adopt a parallel-stranded arrangement of the two G-tracts via a double-chain-reversal loop.[14,45−47]

Longer Loops Do Not Necessarily Lead to Less Stable G-Quadruplex Structures. Prior studies on the effects of loop length on the conformation and stability of G-quadruplexes have generally agreed that short loops (≤2 nt) show a preference for the propeller configuration[14,15,17,20] and that longer loops tend to have a destabilizing influence on G-quadruplex structures.[14,15,18−20,22] It should be noted that in these studies, the long loops that were investigated did not contain any explicit stabilizing interactions, which might account for their destabilizing nature. It has generally been accepted that a stable G-quadruplex structure should have loops that contain no more than seven nucleotides.[37] Recently we described the structure of a parallel G-quadruplex comprising a nine-nucleotide central propeller loop, in which interactions between sections of the long loop and capping elements of the G-tetrad core contribute toward its overall stability.[47] Here we have shown that a long loop (in the form of a duplex stem) by

dx.doi.org/10.1021/bi401161a | *Biochemistry* 2014, 53, 247−257

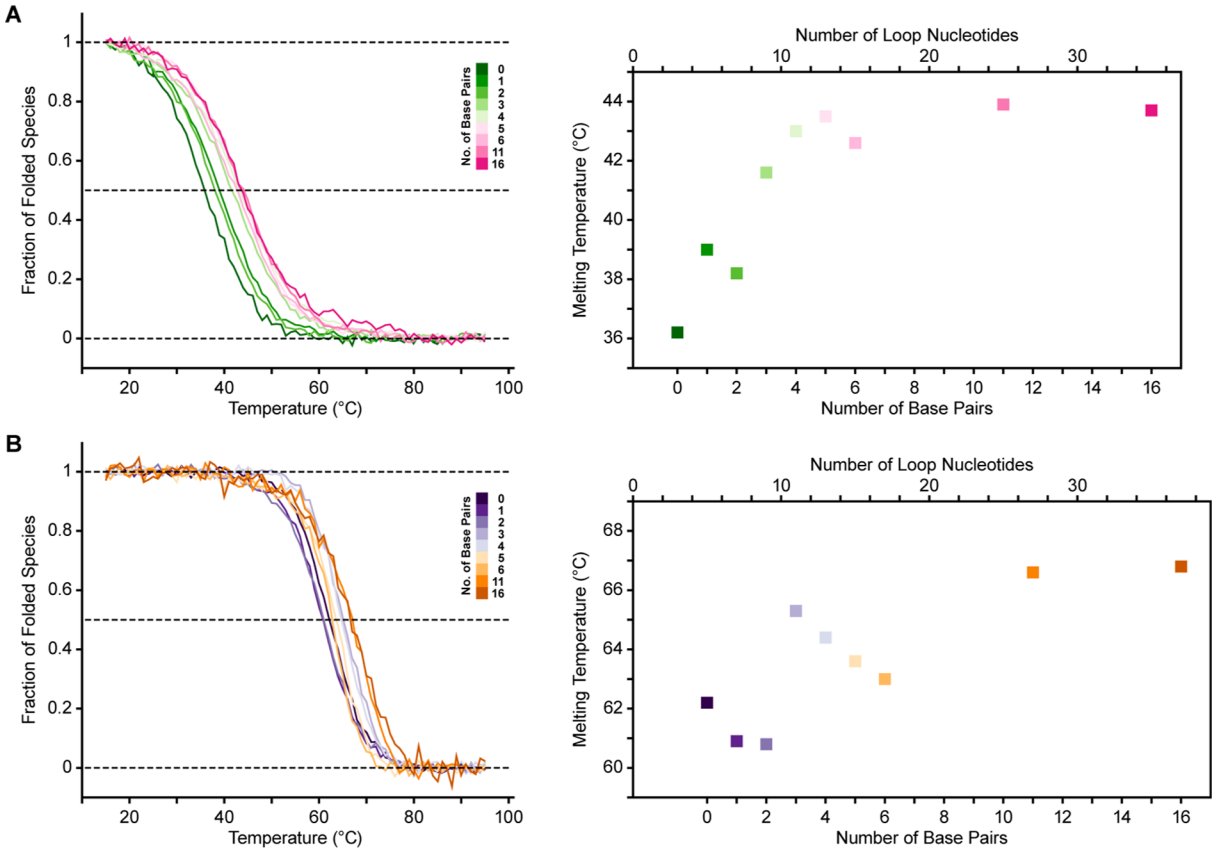

Figure 7. Stability of quadruplex–duplex hybrids comprising different stem lengths. (A) Folding curves (left; color-coded on the top right corner) and melting temperatures (right) for Construct I across various stem lengths, as monitored at 295 nm. (B) Folding curves (left; color-coded on the top right corner) and melting temperatures (right) for Construct II across various stem lengths, as monitored at 262 nm.

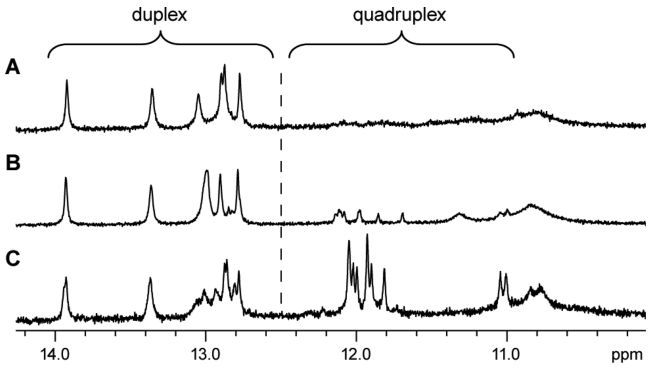

Figure 8. 1D imino proton NMR spectra of Construct I consisting of a single-nucleotide bulge at (A) the 5′-side (*W2C-6bp[+T7]*), (B) the 3′-side (*W2C-6bp[+T21]*), and (C) both the 5′-side and the 3′-side (*W2C-6bp[+T7/+T22]*) of the duplex stem adjoining the quadruplex.

itself can also exert a stabilizing influence on a quadruplex, particularly, with respect to a nonstructured loop of the same length: for Construct I, the desired quadruplex topology was no longer the major form with a nonstructured loop of five nucleotides or longer; for Construct II, higher quadruplex stability was observed for complexes containing two or more base pairs in the duplex stem, with respect to those containing a nonstructured loop of the same length.

Contexts at the Junctions Influence the Stability and Uniformity of Quadruplex–Duplex Hybrids. We have shown that variability at the base-pair step immediately adjoining the quadruplex–duplex junction can alter the melting temperature of the complex to a significant extent, which differs in the case of Construct I and Construct II. For Construct II, the outcome is of a more predictable nature: Watson–Crick G·C base pairs are slightly more stable than A·T base pairs in general. On the other hand, the large differences in stability observed for Construct I suggest that other factors could be in play at the stacked quadruplex–duplex interface. The investigation is by no means exhaustive and is only intended to provide a gauge of the extent of fluctuations in stability associated with changes in base-pair composition near the junction.

We also explored the addition of bulges onto both sides of the quadruplex–duplex junction. For a junction involving continual stacking of bases, as is the case in Construct I, a single bulge at either side of the junction is detrimental to the adoption of a single G-quadruplex topology for the quadruplex–duplex hybrid. It is interesting to note that a bulge at the 3′-side of the duplex stem poses a less severe effect than does a bulge at the 5′-side. The presence of single-nucleotide bulges on both sides of the junction, which could either be flipped out[31] or stacked[30,48] at the quadruplex–duplex interface, restored the desired G-quadruplex topology as the major species but reduced the stability of the complex nonetheless. In contrast, in the case of the propeller duplex stem–loop (Construct II), bulges (up to three nucleotides on either/both sides of the quadruplex–duplex junction) did not seem to adversely affect the formation of the desired G-quadruplex topology, even when the bulge sizes at both sides of the junction are not the same. This could partly have been

dx.doi.org/10.1021/bi401161a | *Biochemistry* 2014, 53, 247–257

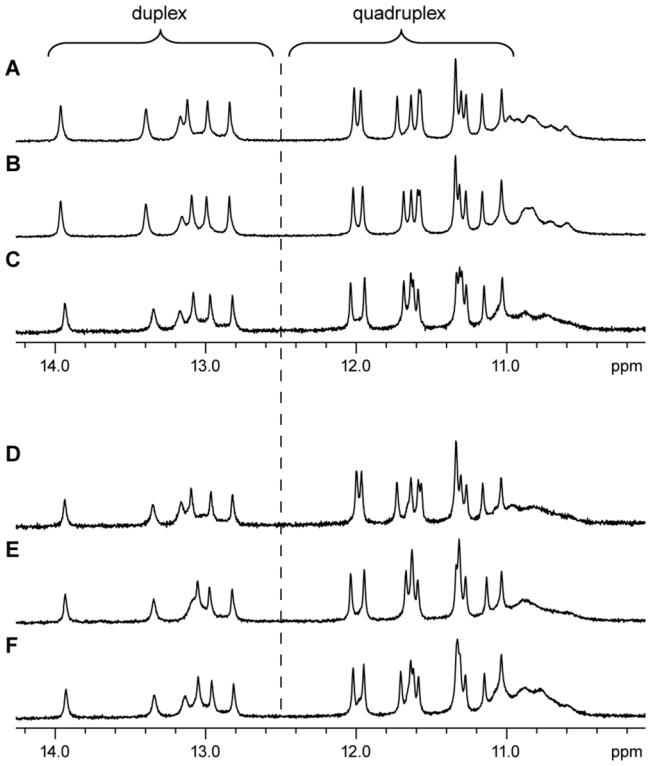

Figure 9. 1D imino proton NMR spectra of Construct II with bulges at the 5′-side and the 3′-side of the duplex stem adjoining the quadruplex: (A) *M2C-6bp[+T11]*; (B) *M2C-6bp[+T26]*; (C) *M2C-6bp[+T11/+T27]*; (D) *M2C-6bp[+T11T12]*; (E) *M2C-6bp-[+T26T27]*; (F) *M2C-6bp[+T11T12/+T28T29]*.

offset by the robust nature of the all-parallel-stranded G-tetrad core. The number of bulge nucleotides on either side of the junction dictates the flexibility and projection of the propeller duplex stem–loop and could potentially be utilized to fine-tune the relative orientation of the duplex and quadruplex helices in the design of DNA nanodevices. It should be noted that the effects of bulge incorporation at the quadruplex–duplex junction for Construct I and Construct II should not be compared directly, since formation of the latter entails a minimum of one bulged nucleotide at both sides of the junction.

Stacking (or Nonstacking) at the Quadruplex–Duplex Interface. We have examined two contrasting modes of quadruplex–duplex connectivity, one involving the continual stacking of bases at the interface (Construct I) and the other involving the disruption of base stacking between the two segments (Construct II). The presence/absence of stacking was reflected in the NMR and CD spectra: (1) for Construct I, base-pair addition/substitution at the junction resulted in considerable changes in the chemical shifts of the tetrad imino protons (Figure 3 and Figure S10 in the Supporting Information), whereas for Construct II the chemical shifts of the tetrad imino protons did not vary much with the addition/substitution of base pair at the quadruplex–duplex junction (Figure 4 and Figure S11 in the Supporting Information); (2) for Construct I, the CD spectrum of the quadruplex–duplex hybrid did not closely match the sum of the spectra of the respective duplex and quadruplex components at ∼250–280 nm, whereas for Construct II the CD spectrum of the quadruplex–duplex hybrid closely matched the sum of the spectra of the respective duplex and quadruplex components. These differences in stacking/nonstacking at the quadruplex–duplex interface are also translated as distinctive trends in the stability/uniformity of the adopted G-quadruplex topology with regard to changes in composition at the junction. Construct I is affected to a greater extent by alterations at the quadruplex–duplex interface (relatively large deviations in melting temperature occur with variation of the base pair at the junction; the introduction of bulges is extremely detrimental to adoption of the desired G-quadruplex topology), whereas Construct II appears to be more refractory to such changes (only slight changes in melting temperature occur with variation of the base pair at the junction; the introduction of bulges does not adversely affect the adoption of the desired G-quadruplex topology). There appears to be little cooperativity between the quadruplex and duplex components in terms of folding/unfolding. For instance in Construct I, their melting transitions did not seem to occur simultaneously (Figure S13 in the Supporting Information). However, such cooperativity could potentially be dependent on the relative placement of the two components; in this study, the duplex-forming elements were situated as contiguous hairpin sequences within the oligonucleotide, whereas the quadruplex-forming elements were situated at the 5′- and 3′-termini, separated by the hairpin sequence. This could have resulted in the higher melting temperature range observed for the hairpin component relative to the quadruplex component.

■ CONCLUSION

Our results show that a duplex stem–loop can exert a stabilizing influence on a quadruplex structure with respect to a nonstructured loop of the same length. Depending on the context, alterations to the quadruplex–duplex junction can substantially affect the conformation and stability of these structures. These findings should be applicable to quadruplex–duplex hybrids comprising similar arrangements of duplex and quadruplex helices and should aid in the future design and prediction of these motifs.

■ ASSOCIATED CONTENT

Supporting Information

NMR and CD spectra and the melting temperatures of various DNA duplex hairpins, quadruplexes, and quadruplex–duplex hybrids. This material is available free of charge via the Internet at http://pubs.acs.org.

■ AUTHOR INFORMATION

Corresponding Author

*Phone: (+65) 6514 1915. E-mail: phantuan@ntu.edu.sg.

Author Contributions

§K.W.L. and Z.J.K. contributed equally to this work.

Funding

This research was supported by grants from the Singapore Ministry of Education and Nanyang Technological University to A.T.P.

Notes

The authors declare no competing financial interest.

■ ACKNOWLEDGMENTS

Z.J.K., a student from Ngee Ann Polytechnic (NP), was on an industrial attachment program supported by NP. We thank Zhen Jie Low for his participation at the early stage of the project.

REFERENCES

(1) Davis, J. T. (2004) G-quartets 40 years later: From 5′-GMP to molecular biology and supramolecular chemistry. *Angew. Chem., Int. Ed. 43*, 668−698.

(2) Burge, S., Parkinson, G. N., Hazel, P., Todd, A. K., and Neidle, S. (2006) Quadruplex DNA: Sequence, topology and structure. *Nucleic Acids Res. 34*, 5402−5415.

(3) Patel, D. J., Phan, A. T., and Kuryavyi, V. (2007) Human telomere, oncogenic promoter and 5′-UTR G-quadruplexes: Diverse higher order DNA and RNA targets for cancer therapeutics. *Nucleic Acids Res. 35*, 7429−7455.

(4) Gellert, M., Lipsett, M. N., and Davies, D. R. (1962) Helix formation by guanylic acid. *Proc. Natl. Acad. Sci. U.S.A. 48*, 2013−2018.

(5) Hoogsteen, K. (1963) The crystal and molecular structure of a hydrogen-bonded complex between 1-methylthymine and 9-methyladenine. *Acta Crystallogr. 16*, 907−916.

(6) Lim, K. W., and Phan, A. T. (2013) Structural basis of DNA quadruplex−duplex junction formation. *Angew. Chem., Int. Ed. 52*, 8566−8569.

(7) Palumbo, S. L., Ebbinghaus, S. W., and Hurley, L. H. (2009) Formation of a unique end-to-end stacked pair of G-quadruplexes in the hTERT core promoter with implications for inhibition of telomerase by G-quadruplex-interactive ligands. *J. Am. Chem. Soc. 131*, 10878−10891.

(8) Huang, Y. C., and Sen, D. (2010) A contractile electronic switch made of DNA. *J. Am. Chem. Soc. 132*, 2663−2671.

(9) Dutta, K., Fujimoto, T., Inoue, M., Miyoshi, D., and Sugimoto, N. (2010) Development of new functional nanostructures consisting of both DNA duplex and quadruplex. *Chem. Commun. 46*, 7772−7774.

(10) Yu, Z. B., Gaerig, V., Cui, Y. X., Kang, H. J., Gokhale, V., Zhao, Y., Hurley, L. H., and Mao, H. B. (2012) Tertiary DNA structure in the single-stranded hTERT promoter fragment unfolds and refolds by parallel pathways via cooperative or sequential events. *J. Am. Chem. Soc. 134*, 5157−5164.

(11) Risitano, A., and Fox, K. R. (2003) The stability of intramolecular DNA quadruplexes with extended loops forming inter- and intra-loop duplexes. *Org. Biomol. Chem. 1*, 1852−1855.

(12) Lane, A. N., Chaires, J. B., Gray, R. D., and Trent, J. O. (2008) Stability and kinetics of G-quadruplex structures. *Nucleic Acids Res. 36*, 5482−5515.

(13) Kumar, N., and Maiti, S. (2008) A thermodynamic overview of naturally occurring intramolecular DNA quadruplexes. *Nucleic Acids Res. 36*, 5610−5622.

(14) Phan, A. T., Modi, Y. S., and Patel, D. J. (2004) Propeller-type parallel-stranded G-quadruplexes in the human *c-myc* promoter. *J. Am. Chem. Soc. 126*, 8710−8716.

(15) Hazel, P., Huppert, J., Balasubramanian, S., and Neidle, S. (2004) Loop-length-dependent folding of G-quadruplexes. *J. Am. Chem. Soc. 126*, 16405−16415.

(16) Risitano, A., and Fox, K. R. (2004) Influence of loop size on the stability of intramolecular DNA quadruplexes. *Nucleic Acids Res. 32*, 2598−2606.

(17) Rachwal, P. A., Brown, T., and Fox, K. R. (2007) Sequence effects of single base loops in intramolecular quadruplex DNA. *FEBS Lett. 581*, 1657−1660.

(18) Rachwal, P. A., Findlow, I. S., Werner, J. M., Brown, T., and Fox, K. R. (2007) Intramolecular DNA quadruplexes with different arrangements of short and long loops. *Nucleic Acids Res. 35*, 4214−4222.

(19) Bugaut, A., and Balasubramanian, S. (2008) A sequence-independent study of the influence of short loop lengths on the stability and topology of intramolecular DNA G-quadruplexes. *Biochemistry 47*, 689−697.

(20) Guédin, A., De Cian, A., Gros, J., Lacroix, L., and Mergny, J. L. (2008) Sequence effects in single-base loops for quadruplexes. *Biochimie 90*, 686−696.

(21) Guédin, A., Alberti, P., and Mergny, J. L. (2009) Stability of intramolecular quadruplexes: Sequence effects in the central loop. *Nucleic Acids Res. 37*, 5559−5567.

(22) Guédin, A., Gros, J., Alberti, P., and Mergny, J. L. (2010) How long is too long? Effects of loop size on G-quadruplex stability. *Nucleic Acids Res. 38*, 7858−7868.

(23) Adrian, M., Heddi, B., and Phan, A. T. (2012) NMR spectroscopy of G-quadruplexes. *Methods 57*, 11−24.

(24) Vorlíčková, M., Kejnovská, I., Bednářová, K., Renčiuk, D., and Kypr, J. (2012) Circular dichroism spectroscopy of DNA: From duplexes to quadruplexes. *Chirality 24*, 691−698.

(25) Cantor, C. R., Warshaw, M. M., and Shapiro, H. (1970) Oligonucleotide interactions. III. Circular dichroism studies of conformation of deoxyoligonucleotides. *Biopolymers 9*, 1059−1077.

(26) Schultze, P., Macaya, R. F., and Feigon, J. (1994) Three-dimensional solution structure of the thrombin-binding DNA aptamer d(GGTTGGTGTGGTTGG). *J. Mol. Biol. 235*, 1532−1547.

(27) Do, N. Q., Lim, K. W., Teo, M. H., Heddi, B., and Phan, A. T. (2011) Stacking of G-quadruplexes: NMR structure of a G-rich oligonucleotide with potential anti-HIV and anticancer activity. *Nucleic Acids Res. 39*, 9448−9457.

(28) Do, N. Q., and Phan, A. T. (2012) Monomer−dimer equilibrium for the 5′−5′ stacking of propeller-type parallel-stranded G-quadruplexes: NMR structural study. *Chem.—Eur. J. 18*, 14752−14759.

(29) Zhu, L. M., Chou, S. H., Xu, J. D., and Reid, B. R. (1995) Structure of a single-cytidine hairpin loop formed by the DNA triplet GCA. *Nat. Struct. Biol. 2*, 1012−1017.

(30) Patel, D. J., Kozlowski, S. A., Marky, L. A., Rice, J. A., Broka, C., Itakura, K., and Breslauer, K. J. (1982) Extra adenosine stacks into the self-complementary d(CGCAGAATTCGCG) duplex in solution. *Biochemistry 21*, 445−451.

(31) Joshua-Tor, L., Rabinovich, D., Hope, H., Frolow, F., Appella, E., and Sussman, J. L. (1988) The three-dimensional structure of a DNA duplex containing looped-out bases. *Nature 334*, 82−84.

(32) Summers, M. F., Byrd, R. A., Gallo, K. A., Samson, C. J., Zon, G., and Egan, W. (1985) Nuclear magnetic resonance and circular dichroism studies of a duplex single-stranded hairpin loop equilibrium for the oligodeoxyribonucleotide sequence d(CGCGATTCGCG). *Nucleic Acids Res. 13*, 6375−6386.

(33) Lim, K. W., Alberti, P., Guédin, A., Lacroix, L., Riou, J. F., Royle, N. J., Mergny, J. L., and Phan, A. T. (2009) Sequence variant $(CTAGGG)_n$ in the human telomere favors a G-quadruplex structure containing a G·C·G·C tetrad. *Nucleic Acids Res. 37*, 6239−6248.

(34) Gray, D. M., Wen, J. D., Gray, C. W., Repges, R., Repges, C., Raabe, G., and Fleischhauer, J. (2008) Measured and calculated CD spectra of G-quartets stacked with the same or opposite polarities. *Chirality 20*, 431−440.

(35) Seeman, N. C. (2010) Nanomaterials based on DNA. *Annu. Rev. Biochem. 79*, 65−87.

(36) Todd, A. K., Johnston, M., and Neidle, S. (2005) Highly prevalent putative quadruplex sequence motifs in human DNA. *Nucleic Acids Res. 33*, 2901−2907.

(37) Huppert, J. L., and Balasubramanian, S. (2005) Prevalence of quadruplexes in the human genome. *Nucleic Acids Res. 33*, 2908−2916.

(38) Xu, Y., Noguchi, Y., and Sugiyama, H. (2006) The new models of the human telomere d[AGGG$(TTAGGG)_3$] in K^+ solution. *Bioorg. Med. Chem. 14*, 5584−5591.

(39) Phan, A. T., Kuryavyi, V., Luu, K. N., and Patel, D. J. (2007) Structure of two intramolecular G-quadruplexes formed by natural human telomere sequences in K^+ solution. *Nucleic Acids Res. 35*, 6517−6525.

(40) Matsugami, A., Xu, Y., Noguchi, Y., Sugiyama, H., and Katahira, M. (2007) Structure of a human telomeric DNA sequence stabilized by 8-bromoguanosine substitutions, as determined by NMR in a K^+ solution. *FEBS J. 274*, 3545−3556.

(41) Okamoto, K., Sannohe, Y., Mashimo, T., Sugiyama, H., and Terazima, M. (2008) G-quadruplex structures of human telomere DNA examined by single molecule FRET and BrG-substitution. *Bioorg. Med. Chem. 16*, 6873−6879.

(42) Webba da Silva, M., Trajkovski, M., Sannohe, Y., Hessari, N. M., Sugiyama, H., and Plavec, J. (2009) Design of a G-quadruplex

topology through glycosidic bond angles. *Angew. Chem., Int. Ed. 48*, 9167−9170.
(43) Yue, D. J. E., Lim, K. W., and Phan, A. T. (2011) Formation of (3 + 1) G-quadruplexes with a long loop by human telomeric DNA spanning five or more repeats. *J. Am. Chem. Soc. 133*, 11462−11465.
(44) Zhou, J., Bourdoncle, A., Rosu, F., Gabelica, V., and Mergny, J. L. (2012) Tri-G-quadruplex: Controlled assembly of a G-quadruplex structure from three G-rich strands. *Angew. Chem., Int. Ed. 51*, 11002−11005.
(45) Kuryavyi, V., Majumdar, A., Shallop, A., Chernichenko, N., Skripkin, E., Jones, R., and Patel, D. J. (2001) A double chain reversal loop and two diagonal loops define the architecture of a unimolecular DNA quadruplex containing a pair of stacked G(*syn*)·G(*syn*)·G(*anti*)·G(*anti*) tetrads flanked by a G·(T-T) triad and a T·T·T triple. *J. Mol. Biol. 310*, 181−194.
(46) Dai, J. X., Dexheimer, T. S., Chen, D., Carver, M., Ambrus, A., Jones, R. A., and Yang, D. Z. (2006) An intramolecular G-quadruplex structure with mixed parallel/antiparallel G-strands formed in the human BCL-2 promoter region in solution. *J. Am. Chem. Soc. 128*, 1096−1098.
(47) Amrane, S., Adrian, M., Heddi, B., Serero, A., Nicolas, A., Mergny, J. L., and Phan, A. T. (2012) Formation of pearl-necklace monomorphic G-quadruplexes in the human CEB25 minisatellite. *J. Am. Chem. Soc. 134*, 5807−5816.
(48) Balkwill, G. D., Garner, T. P., Williams, H. E. L., and Searle, M. S. (2009) Folding topology of a bimolecular DNA quadruplex containing a stable mini-hairpin motif within the diagonal loop. *J. Mol. Biol. 385*, 1600−1615.